ELSEVIER

J. Non-Newtonian Fluid Mech. 116 (2003) 55–70

Journal of Non-Newtonian Fluid Mechanics

www.elsevier.com/locate/jnnfm

Stretching of a straight electrically charged viscoelastic jet

J.J. Feng*

The Levich Institute for Physicochemical Hydrodynamics, City College of the City University of New York, New York, NY 10031, USA

Received 23 August 2002; received in revised form 28 March 2003

Abstract

A charged polymer jet may be accelerated and stretched by an external electric field, and this process is relevant to electrospinning for making nanofibers. The stretching of an electrified jet is governed by the interplay among electrostatics, fluid mechanics and rheology, and the role of viscoelasticity has not been systematically explored before. This paper presents a slender-body theory for the stretching of a straight charged jet of Giesekus fluid. Results show strain-hardening as the most influential rheological property. It causes the tensile force to rise at the start, which enhances stretching of the jet. Further downstream, however, the higher elongational viscosity tends to suppress jet stretching. In the end, strain-hardening leads to thicker fibers. This confirms the main result of a previous study using empirical rheological models. The behavior of the electrically driven jet forms an interesting contrast to that in conventional fiber spinning.
© 2003 Published by Elsevier B.V.

Keywords: Electrospinning; Uniaxial extension; Slender-body theory; Giesekus model

1. Introduction

The idea of using an electric field to spin fibers from a charged polymer melt or solution was conceived in the 1930s. Electrospinning, as the process is called, has seen a dramatic revival of interest in recent years because of its potential to produce ultra-fine nanofibers with sub-micrometer diameters [1]. Though easily realizable in the laboratory, electrospinning is a complex phenomenon to analyze because of the coupling between the electric field and the deformation of the fluid, the latter in turn determined by the rheology of the material. Typically, electrospinning has two stages. In the first, the polymer jet issues from a nozzle and thins steadily and smoothly downstream. In the second stage, the thin thread becomes unstable to a non-axisymmetric instability and spirals violently in large loops. For stage one, Hohman et al. [2] presented a slender-body theory for Newtonian fluids. Spivak and Dzenis [3] introduced a power-law

* Tel.: +1-212-650-6844; fax: +1-212-650-6835.
E-mail address: feng@levdec.engr.ccny.cuny.edu (J.J. Feng).
URL: http://www.lisgi1.engr.ccny.cuny.edu.

0377-0257/$ – see front matter © 2003 Published by Elsevier B.V.
doi:10.1016/S0377-0257(03)00173-3

viscosity. Reneker et al. [4] modeled the viscoelasticity of the jet by a linear Maxwell equation. For stage two, Hohman et al. [2] and Reneker and coworkers [4,5] developed instability theories for Newtonian and linear Maxwell fluids, respectively. None of these theories accounted for the nonlinear viscoelasticity that undoubtedly arises during large-strain stretching of the polymer.

In an attempt to understand the role of rheology, Feng [6] introduced empirical models for the elongational viscosity into the slender-body theory of [2] for the steady stretching in stage one. Two special cases were considered. The first is the small-Deborah-number limit where the polymer molecules equilibrate instantaneously with respect to the local strain rate. Then the rheology reduces to a generalized Newtonian elongational viscosity that may include both extension-thinning and thickening. In the second case, an empirical expression for a strain-dependent Trouton ratio is used to incorporate strain-hardening:

$$\frac{\bar{\eta}^+}{3\eta_s} = \begin{cases} \exp\left\{p\left[1-\cos\left(\dfrac{\gamma^2}{\gamma_s^2}\pi\right)\right]\right\} & \text{if } \gamma \le \gamma_s, \\ \exp(2p) & \text{if } \gamma > \gamma_s, \end{cases} \tag{1}$$

where η_s is the viscosity of a Newtonian solvent, γ_s is the strain at which a steady-state extensional viscosity is attained, and the parameter p determines the steady-state Trouton ratio. Inspired by the data of Tirtaatmadja and Sridhar [7] for dilute Boger fluids, this equation is a crude representation of the memory effect and does not reflect certain aspects of the rheology of concentrated solutions and melts. For instance, the strain rate is not included explicitly, and hence no account is taken of the Deborah number. In real polymer melts, $\bar{\eta}^+$ depends not only on the accumulated strain γ but also on the strain rate or Deborah number. The latter determines the point of onset and the magnitude of strain-hardening ([8], pp. 134–136). The rationale for the empirical approach in [6] was to treat the viscous and elastic aspects of the rheology separately so as to simplify the calculation and data analysis.

In this paper, we advance a more rational approach by incorporating the Giesekus constitutive equation into the slender-body theory. The choice of the Giesekus model is based on two considerations. First, it is molecularly-based rather than phenomenological; it models packed polymer chains experiencing anisotropic Brownian and viscous forces [9]. Second and more importantly, the Giesekus model strikes a good balance between simplicity and satisfactory prediction for elongational rheology. Khan and Larson [10] compared the predictions of various models with measurements on a linear HDPE melt for step shear, startup of uniaxial elongation and step biaxial extension. Tirtaatmadja and Sridhar [11] benchmarked an array of models using startup of elongation for Boger fluids. Both studies have reached similar conclusions. Quasi-linear models such as the upper-convected Maxwell, Oldroyd-B and White–Metzner models predict unbounded growth of the elongational viscosity while the measurements show a plateau at large strains. The Giesekus model, arguably the simplest non-linear extension of the quasi-linear models, correctly predicts the plateau, and "can describe the shear damping function and elongational viscosity of an unbranched melt, such as HDPE, quite accurately" [10]. Its disadvantage, as compared with the more sophisticated Larson and Phan–Thien–Tanner models, is in underpredicting the strain softening in the biaxial damping function. Fortunately, this is of little concern in our context. One caveat is that electrospinning may incur exceedingly high strain rates ($\sim 10^3\,\mathrm{s}^{-1}$; see parameter values in Section 4), at which little is known of the performance of any of the constitutive equations.

As in [6], this paper is limited to the steady thinning of a straight electrified jet, relevant only to stage one of electrospinning. For convenience, however, we refer to this process simply as electrospinning for the rest of the paper. In a real electrospinning experiment, stage two is probably more significant in reducing

the fiber diameter to nanometer scale. Nonetheless, the process studied here is important in that it not only contributes directly to the thinning of the fiber, but also establishes the conditions for the onset of stage two.

2. Formulation of the problem

We consider a downward polymer jet in an electric field (Fig. 1). The deformation of the fluid is determined by a balance among the electrostatic forces, gravity, surface tension, viscoelastic force and inertia. We assume that the fluid is a leaky dielectric with charges only on the surface [12], that the process is steady in an Eulerian sense, and that the slope of the jet surface is small. Then a 1D slender-body model can be established based on mass conservation, momentum and electric charge balance, and Coulomb's law. All variables are assumed to be uniform on the cross-section of the jet, and to vary only along z, whose origin is at the nozzle.

In experiments, the slope of the jet surface can be fairly large near the nozzle [2], thus posing a difficulty for a 1D model. On the other hand, 1D models have been applied to numerous problems where the gradient along the axial direction may not be small at all locations. Examples include the detachment of a Newtonian drop from an orifice [13], breakup of a Newtonian liquid bridge [14] and the die-swell of a viscoelastic fluid in conventional fiber spinning [15]. In these cases, the 1D models have been confirmed, by 2D computations or experiments, to give accurate predictions beyond their expected range of applicability [6]. For electrospinning, such validation is not yet available. A plausible treatment is to attach a 1D jet to a 2D Taylor cone [16,17]. Unfortunately, this leads to a voltage-independent "universal current" that does not agree with electrospinning experiments [2]. Without carrying out a 2D simulation of jet initiation, we will apply the slender-body theory upstream to the nozzle, as has been done in previous electrospinning models [2,6].

2.1. Governing equations

The governing equations for jet radius R, axial velocity v, axial electric field E and surface charge density σ have been derived in [2,6]:

$$\pi R^2 v = Q, \tag{2}$$

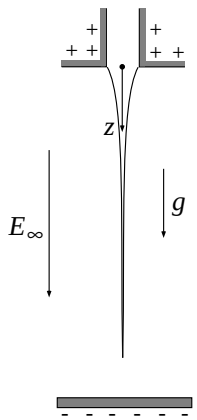

Fig. 1. Schematic of the setup for electrospinning.

$$\pi R^2 KE + 2\pi R v\sigma = I, \tag{3}$$

$$\rho v v' = \rho g + \frac{T'}{\pi R^2} + \frac{\gamma R'}{R^2} + \frac{\sigma\sigma'}{\bar{\epsilon}} + (\epsilon - \bar{\epsilon})EE' + \frac{2\sigma E}{R}, \tag{4}$$

$$E = E_\infty - \ln\chi\left[\frac{(\sigma R)'}{\bar{\epsilon}} - \frac{\beta}{2}(ER^2)''\right], \tag{5}$$

where Q is the constant volume flow rate, K the conductivity of the liquid, I the constant total current in the jet and ρ the fluid density. T is the tensile force in the jet, γ is the surface tension and ϵ and $\bar{\epsilon}$ are the dielectric constants of the jet and the ambient air, respectively. E_∞ is the externally imposed constant field, and χ is the "aspect ratio" of the jet (=length L/initial radius R_0), and $\beta = \epsilon/\bar{\epsilon} - 1$. The prime indicates derivatives with respect to z.

The tensile force $T = \pi R^2(\tau_{zz} - \tau_{rr})$ is related to the strain rate via a constitutive equation, for which we use the Giesekus model [8,9]:

$$\boldsymbol{\tau} = \boldsymbol{\tau}_\mathrm{p} + \eta_\mathrm{s}(\nabla\boldsymbol{v} + \nabla\boldsymbol{v}^\mathrm{T}), \tag{6}$$

$$\boldsymbol{\tau}_\mathrm{p} + \lambda\boldsymbol{\tau}_{\mathrm{p}(1)} + \alpha\frac{\lambda}{\eta_\mathrm{p}}\boldsymbol{\tau}_\mathrm{p}\cdot\boldsymbol{\tau}_\mathrm{p} = \eta_\mathrm{p}(\nabla\boldsymbol{v} + \nabla\boldsymbol{v}^\mathrm{T}), \tag{7}$$

where the subscript (1) denotes the upper convected derivative, α is the mobility factor, λ is the relaxation time, and η_s and η_p are viscosities due to the solvent and the polymer, respectively. For the non-uniform uniaxial extension considered here (see [8], p. 382 for the strain-rate tensor), Eq. (7) reduces to two scalar equations for the polymer normal stress components:

$$\tau_{\mathrm{p}rr} + \lambda(v\tau'_{\mathrm{p}rr} + v'\tau_{\mathrm{p}rr}) + \alpha\frac{\lambda}{\eta_\mathrm{p}}\tau^2_{\mathrm{p}rr} = -\eta_\mathrm{p}v', \tag{8}$$

$$\tau_{\mathrm{p}zz} + \lambda(v\tau'_{\mathrm{p}zz} - 2v'\tau_{\mathrm{p}zz}) + \alpha\frac{\lambda}{\eta_\mathrm{p}}\tau^2_{\mathrm{p}zz} = 2\eta_\mathrm{p}v'. \tag{9}$$

Now Eqs. (2)–(5), (8) and (9) determine the six unknown functions $R(z)$, $v(z)$, $E(z)$, $\sigma(z)$, $\tau_{\mathrm{p}rr}(z)$ and $\tau_{\mathrm{p}zz}(z)$. Note that Q and I have to be input as parameters. In an electrospinning experiment, the control parameter is typically the external field E_∞, which determines Q and I for a particular experimental device. Having to specify Q and I independently is a trade-off for neglecting details of the experimental setup, which may have strong effects on the dynamics of the jet [2].

If we scale $R(z)$, $v(z)$, $E(z)$, $\sigma(z)$, $\tau_{\mathrm{p}rr}(z)$ and $\tau_{\mathrm{p}zz}(z)$, respectively, by R_0 (the radius at the origin of the jet just outside the nozzle), $v_0 = Q/(\pi R_0^2)$, $E_0 = I/(\pi R_0^2 K)$, $\sigma_0 = \bar{\epsilon}E_0$ and $\tau_0 = \eta_0 v_0/R_0$ with $\eta_0 = \eta_\mathrm{s} + \eta_\mathrm{p}$, and scale z by R_0, the governing equations can be made dimensionless (we use the same symbols for brevity):

$$R^2 v = 1, \tag{10}$$

$$ER^2 + PeRv\sigma = 1, \tag{11}$$

$$vv' = \frac{1}{Fr} + \frac{3(1-r_\eta)}{Re}\frac{(R^2v')'}{R^2} + \frac{1}{Re}\frac{T'_\mathrm{p}}{R^2} + \frac{1}{We}\frac{R'}{R^2} + \mathcal{E}\left(\sigma\sigma' + \beta EE' + \frac{2E\sigma}{R}\right), \tag{12}$$

$$E = E_\infty - \ln\ \chi[(\sigma R)' - \tfrac{1}{2}\beta(ER^2)''], \tag{13}$$

$$\tau_{prr} + De(v\tau'_{prr} + v'\tau_{prr}) + \alpha\frac{De}{r_\eta}\tau^2_{prr} = -r_\eta v', \tag{14}$$

$$\tau_{pzz} + De(v\tau'_{pzz} - 2v'\tau_{pzz}) + \alpha\frac{De}{r_\eta}\tau^2_{pzz} = 2r_\eta v', \tag{15}$$

where $T_p = R^2 N_1 = R^2(\tau_{pzz} - \tau_{prr})$ is the dimensionless tensile force due to the polymer and N_1 is the first normal stress difference of the polymer. The dimensionless groups are:

$$Pe = \frac{2\bar{\epsilon}v_0}{KR_0} \quad \text{(electric Peclet number)},$$

$$Fr = \frac{v_0^2}{gR_0} \quad \text{(Froude number)},$$

$$Re = \frac{\rho v_0 R_0}{\eta_0} \quad \text{(Reynolds number)},$$

$$We = \frac{\rho v_0^2 R_0}{\gamma} \quad \text{(Weber number)},$$

$$\mathcal{E} = \frac{\bar{\epsilon}E_0^2}{\rho v_0^2},$$

$$\beta = \frac{\epsilon}{\bar{\epsilon}} - 1,$$

$$\chi = \frac{L}{R_0} \quad \text{(aspect ratio)},$$

$$De = \frac{\lambda v_0}{R_0} \quad \text{(Deborah number)},$$

$$r_\eta = \frac{\eta_p}{\eta_0} \quad \text{(viscosity ratio)}.$$

2.2. Boundary conditions

Eliminating v and σ among Eqs. (10)–(15), we obtain two second-order ordinary differential equations (ODEs) for R and E and two first-order ODEs for the polymer stress components. Six boundary conditions are required. At the lower end of the jet, the asymptotic scaling $R \sim z^{-1/4}$ prevails. This was first derived by Kirichenko et al. [18] for an inviscid jet, but can be easily shown to hold for viscous and viscoelastic fluids as well. As $z \to \infty$, $R \to 0$. Eqs. (10) and (11) imply $v = R^{-2}$ and $\sigma \sim (Rv)^{-1} \sim R \to 0$. Thus, the electric field becomes uniform $E = E_\infty$ from Eq. (13), and of the three terms of electrostatic forces in Eq. (12), only $2E\sigma/R \sim E_\infty$ remains finite. The solvent and polymer tensile force terms and the surface tension term all vanish (to be confirmed a posteriori), while gravity remains finite. Thus, the

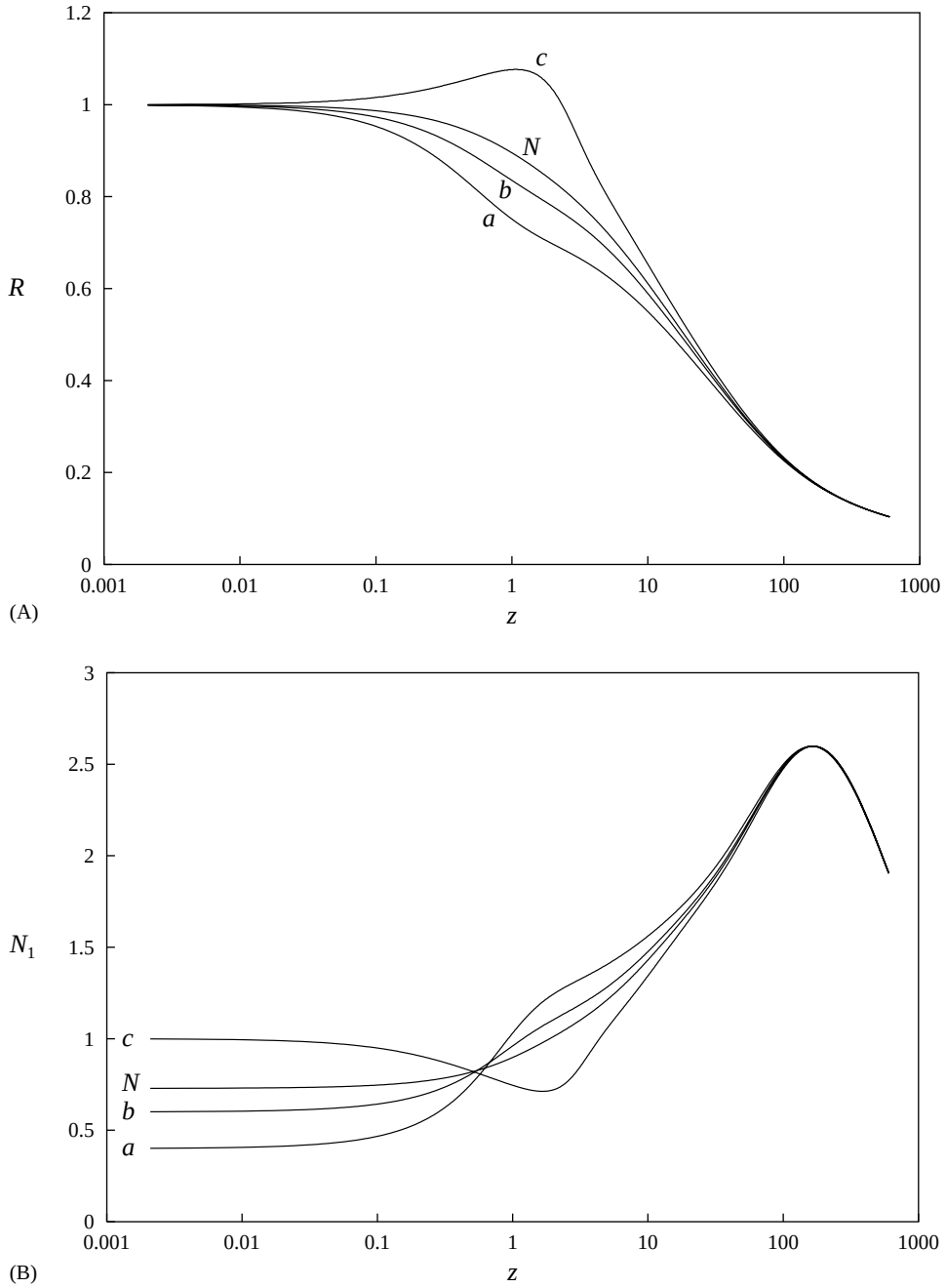

Fig. 2. Effects of the stress boundary condition on (A) jet radius $R(z)$ and (B) normal stress difference $N_1(z) = \tau_{pzz}(z) - \tau_{prr}(z)$. For curves a, b and c, $\tau_{prr}(0) = -0.13$, -0.20 and -0.33 with $\tau_{pzz}(0)/\tau_{prr}(0) = -2$. Curve N corresponds to the Newtonian condition in Eqs. (20) and (21).

inertia on the left-hand-side has to be finite also: $vv' = -2R^{-5}R' = \mathrm{O}(1)$, which leads to the scaling $R \sim z^{-1/4}$. Now we can verify that the constitutive equations revert to Newtonian since $v' \sim z^{-1/2} \to 0$. Then the tensile force terms scale as $z^{-3/2}$ and the surface tension as $z^{-3/4}$, both negligible as compared to the finite gravity and tangential electric force. Thus, we have the following exit conditions at $z = \chi$:

$$R + 4zR' = 0, \tag{16}$$

$$E = E_\infty. \tag{17}$$

As is usually the case with 1D models, the upstream boundary condition is a delicate issue. Following previous work [13,15], we use conditions at the nozzle as entrance conditions for the 1D model even though $|R'|$ may not be small there:

$$R(0) = 1. \tag{18}$$

An issue specific to electrospinning is the upstream condition $E(0)$. Feng [6] showed that the influence of $E(0)$ is limited to a tiny layer below the nozzle whose thickness is a few percent of R_0. Thus, $E(0)$ is assigned some value E_0 so as to avoid a sharp gradient inside the layer:

$$E(0) = E_0. \tag{19}$$

This phenomenology compensates for not accounting for the upstream charges which define $E(0)$ in reality. In the same vein, $\tau_{prr}(0)$ and $\tau_{pzz}(0)$ are determined by the upstream deformation history. Previous work on conventional fiber spinning has either specified the stress at the spinneret [19,20] or postulated a deformation history [21]. We assume that the shear inside the nozzle is ineffective in stretching polymer molecules as compared with the elongation downstream, such that the stress at $z = 0$ is purely Newtonian:

$$\tau_{prr} = -r_\eta v' = 2r_\eta \frac{R'}{R^3}, \tag{20}$$

$$\tau_{pzz} = -2\tau_{prr}. \tag{21}$$

Numerical experiments show that the prediction of the model is rather insensitive to the stress boundary conditions. As an example, Fig. 2 compares results computed using various values of $\tau_{prr}(0)$ while keeping $\tau_{pzz}(0) = -2\tau_{prr}(0)$. The influence of the initial stress is limited to roughly a distance of $10R_0$ downstream. In particular, the final fiber radius is little affected. This is reminiscent of conventional fiber spinning where τ_{prr} quickly drops toward zero downstream regardless of its initial value [19]. Also notable is that a $\tau_{prr}(0)$ that is too large or too small causes under- or overshoots in the profiles, and the "Newtonian conditions" (Eqs. (20) and (21)) apparently give the most reasonable results.

The six coupled ODEs are discretized on a non-uniform grid, with denser nodes near the nozzle to resolve the larger gradients, and solved using a relaxation method [22]. Convergence with grid size has been confirmed by grid refinement.

3. Numerical results

It is useful to review briefly the rheological predictions of the Giesekus model. For $\alpha > 0$, a steady state is always achieved in uniaxial elongation, with an elongational viscosity that increases with the extension rate (extension-thickening) [8]. Fig. 3 plots the transient elongational viscosity $\bar{\eta}^+$ after startup

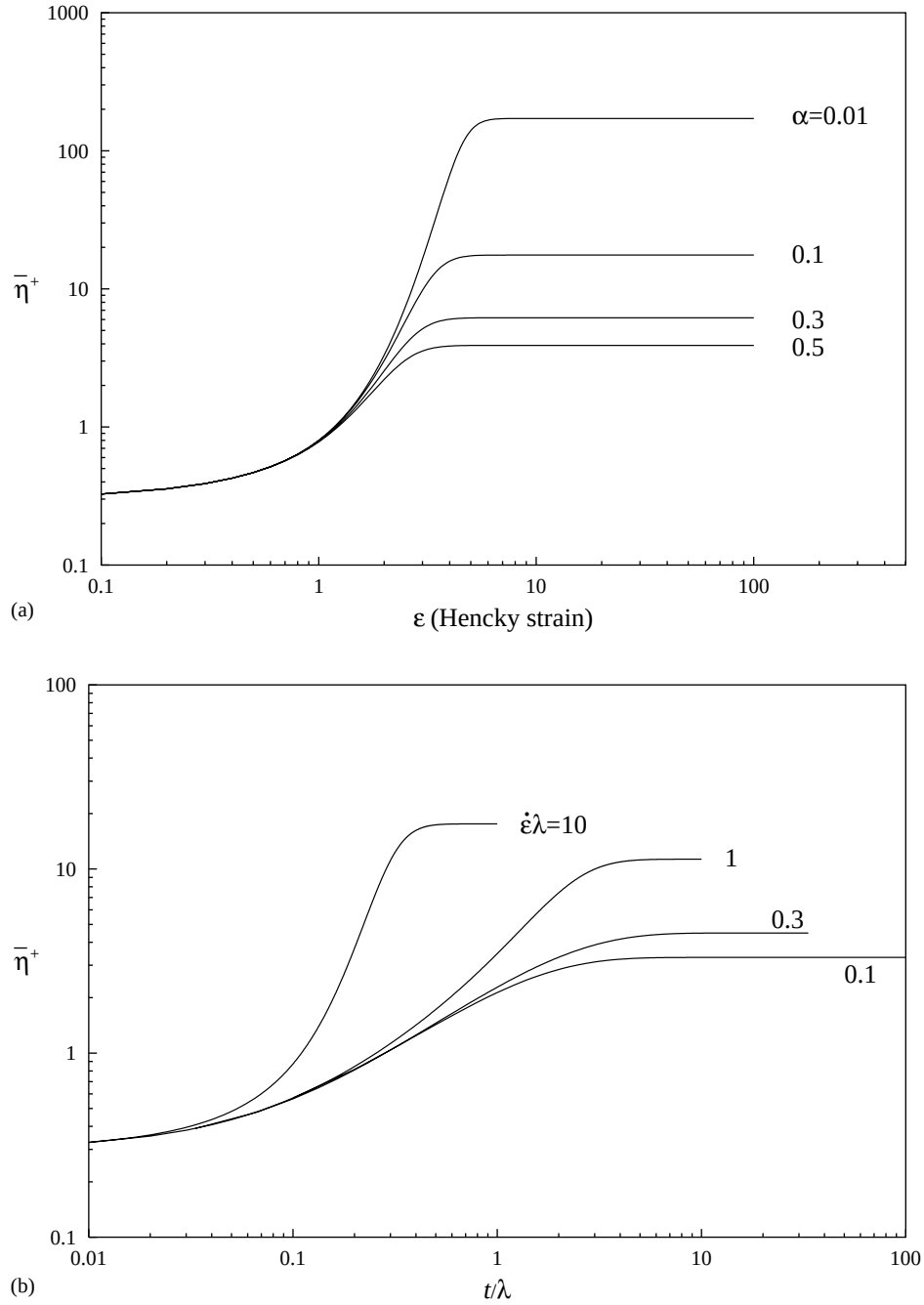

Fig. 3. Transient elongational viscosity of a Giesekus fluid after startup of uniaxial extension. The Hencky strain $\varepsilon = \dot{\varepsilon}t$, and $\bar{\eta}^+$ is made dimensionless by η_0: (a) effects of varying α with $\dot{\varepsilon}\lambda = 10$ and $r_\eta = 0.9$; (b) effects of varying $\dot{\varepsilon}\lambda$ with $\alpha = 0.1$ and $r_\eta = 0.9$.

of a uniaxial extension at a constant rate $\dot{\varepsilon}$. For a small α and/or a large $\dot{\varepsilon}\lambda$, $\bar{\eta}^+$ rises steeply as the molecules transform from a coiled to a stretched state. This behavior, known as strain-hardening, is typical of polymer solutions and melts [8]. As α increases, the degree of strain-hardening decreases although it onsets at more or less the same Hencky strain (Fig. 3(a)). This behavior has been reproduced by the empirical Eq. (1) with a decreasing p (cf. Fig. 13 of [6]). Fig. 3(b), on the other hand, represents new rheology not contained in Eq. (1). With increasing extension rate $\dot{\varepsilon}$, not only is the viscosity plateau elevated (extension-thickening), but the onset of strain-hardening occurs at earlier times. The former occurs in reality at smaller $\dot{\varepsilon}$, and is followed by extension-thinning at higher $\dot{\varepsilon}$ [23]. The latter is a hallmark of nonlinear viscoelasticity, true of all published measurements of melts and concentrated solutions [10,8].

Fig. 4 shows a typical solution for the following parameter values: $\alpha = 0.01$, $De = 10$, $r_\eta = 0.9$, $\chi = 600$, $\beta = 40$, $Re = 2.5 \times 10^{-3}$, $We = 0.1$, $Fr = 0.1$, $Pe = 0.1$, $\mathcal{E} = 1$ and $E_\infty = 0.1$. The same qualitative features prevail over wide ranges of the parameters. According to Fig. 4(a), most of the thinning of the jet occurs at the nozzle; $|R'|$ is maximum at $z = 0$ and relaxes gradually toward zero downstream. In fact, $R'(z = 0) = -0.23$ appears to violate the precondition for a slender-body theory: $|R'| \ll 1$. Yet, slender-body models have performed remarkably well in problems with much greater axial gradients [13,14]. Both E and σ rise at the beginning, reach their respective peaks and then relax downstream. The maximum E occurs very close to the nozzle and is shown in the inset in Fig. 4(b). The key to understand these features is to realize that they are interconnected. At the nozzle, the shrinking cross-section area reduces the amount of charges that can be conducted. Charge conservation demands a higher rate of convection and hence a rising surface charge density σ. The charges then lead to an increase in the axial field E. As the jet becomes thinner further downstream, the increasing jet speed v reduces σ and brings about the decline in $|R'|$ and E as well. For these parameters, the tensile force $T(z)$ decreases monotonically along the fiber (Fig. 4(c)), as is characteristic of the regime of "mild stretching". From Eq. (12), therefore, T acts to resist the acceleration and extension of the fiber. For shorter and more conducting jets, "severe stretching" may occur in which $T(z)$ has a humped shape. Detailed discussion of these two regimes is given by Feng [6].

The electrically driven stretching of the jet forms an interesting contrast to the mechanical stretching in conventional fiber spinning. First, there is no die swell in electrospinning. Not having accounted for the detailed deformation history upstream, our 1D model of course precludes die swell a priori. But even electrospinning experiments do not show die swell; instead a Taylor cone forms at the nozzle with rapid and monotonic thinning of the jet [24]. Indeed, this difference is partly responsible for the much thinner fibers produced by electrospinning. If we take die swell to be a manifestation of the recoil of extended molecules upon exiting the spinneret [25], then it is easily understood how electrostatic forces, acting mostly on the free surface, continue to stress the jet and thus inhibit the elastic recovery. Another fundamental difference between conventional fiber spinning and electrospinning is that the former applies the "pulling force" locally at the wind-up spool while the latter exerts a distributed force. Thus, in the former the total tensile force T remains more or less constant throughout the fiber [20], while it generally decreases along z in the latter (Fig. 4(c)). In conventional fiber spinning, therefore, the normal stress difference N_1 increases monotonically downstream as the fiber becomes thinner. In electrospinning, on the other hand, N_1 typically has a humped shape. The effect of this on $R(z)$ is evident in Fig. 4(a), where we have replotted the 1D calculations of Fisher and Denn [20] of conventional fiber spinning using a White-Metzner model, as well as experimental data for isothermal spinning of polystyrene. When electrically driven, the thinning of the fiber occurs mostly at the nozzle. In conventional spinning, on the other hand, the rate of thinning is sustained over the entire length of the fiber.

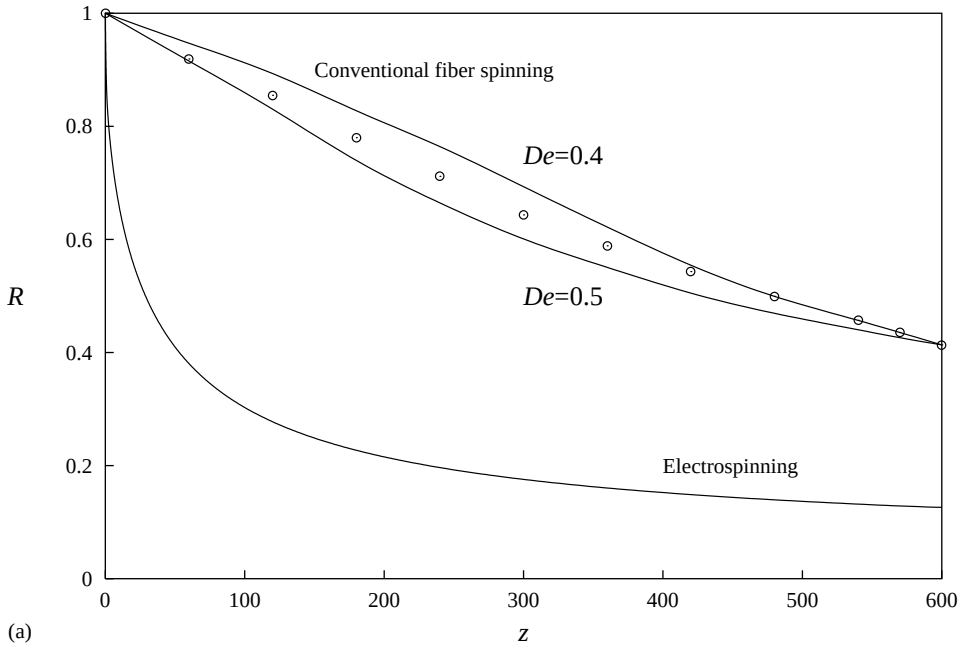

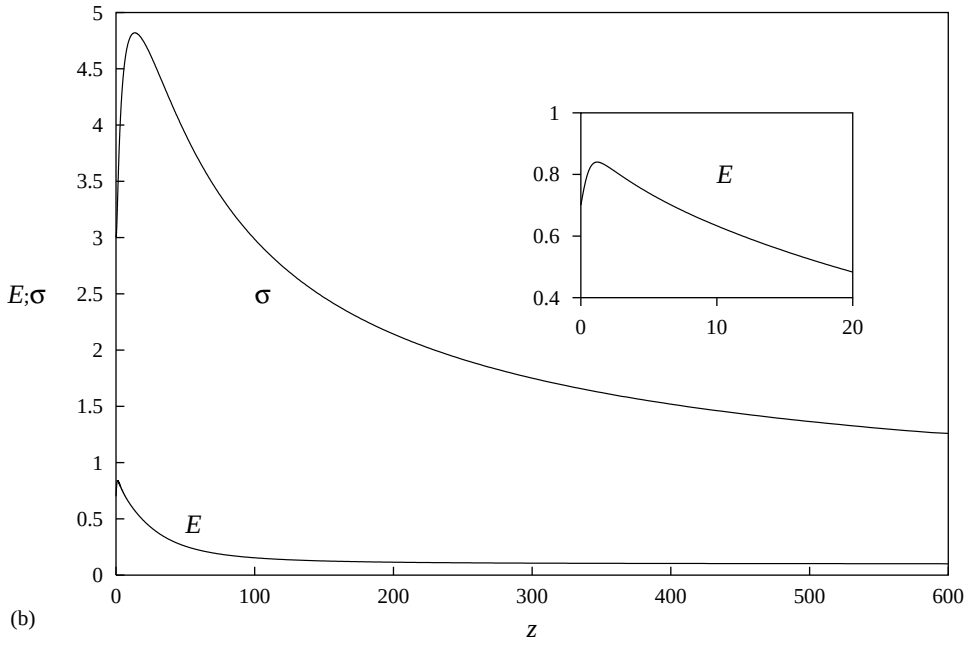

Fig. 4. Typical profiles predicted by the 1D theory for (a) R; (b) E and σ; (c) T. The parameters are: $\alpha = 0.01$, $De = 10$, $r_\eta = 0.9$, $\chi = 600$, $\beta = 40$, $Re = 2.5 \times 10^{-3}$, $We = 0.1$, $Fr = 0.1$, $Pe = 0.1$, $\mathcal{E} = 1$ and $E_\infty = 0.1$. The $R(z)$ profile is compared with experimental data (circles) and calculations for conventional fiber spinning [20], which used the White–Metzner model at a draw ratio of 5.85 and two Deborah numbers.

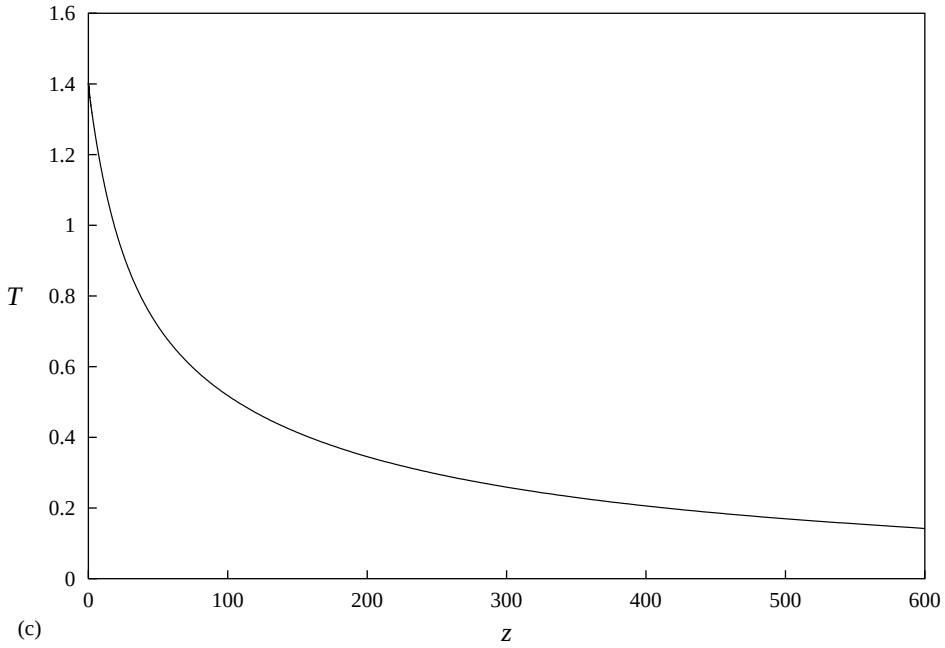

Fig. 4. (*Continued*).

To elucidate the role of rheology in our 1D theory, we examine the effects of the parameters in the Giesekus model: α, *De* and r_η. Fig. 5 compares the thinning curves $R(z)$ and polymer tensile force profile $T_\mathrm{p}(z)$ for several values of α. With increasing α, the thinning of the jet is suppressed initially, within roughly $3R_0$ from the nozzle (see inset in Fig. 5(a)). Further downstream, the trend is reversed and eventually thinner fibers are produced for larger α. This behavior is caused by strain-hardening, and can be explained via the polymer tensile force T_p (Fig. 5(b)). Referring to Fig. 3(a), smaller α gives rise to greater strain-hardening. For $\alpha = 0.01$, this effect is so strong as to overcome the shrinking cross-section area and produce an initial rise in T_p, which, through Eq. (12), promotes stretching and thinning at the beginning of the jet. This effect contradicts our intuition that the more viscous the fluid is, the less it will stretch. The key to this "paradox" is the difference illustrated in Fig. 4(a). The role of $T_\mathrm{p}(z)$ in electrospinning is dictated by the distributive nature of the electrostatic force, while the above intuition derives from more familiar situations of mechanical stretching.

Further downstream, T_p has to decrease owing again to the distributive nature of the electrostatic force. Now the elevated elongational viscosity for smaller α implies a steeper decline in T_p, which suppresses stretching of the jet as is evident in Fig. 5(a). Notably, the trend in Fig. 5 is the same as previously predicted [6] using the empirical Trouton ratio of Eq. (1) fitted to filament stretching experiments of Tirtaatmadja and Sridhar [7]. This is not surprising since, as mentioned in relation to Fig. 3(a), the empirical constitutive equation has embodied strain-hardening, albeit in an ad hoc fashion.

The effect of increasing *De* is to enhance stretching at the beginning and suppress it further downstream (Fig. 6). This is a direct consequence of Fig. 3(b) which shows earlier onset of strain-hardening at higher *De*. One should be cautious, however, since the nominal Deborah number $De = \lambda v_0/R_0$ does not reflect the local rate of extension v', and Fig. 6 does not correspond to a startup of elongation at a constant $\dot{\varepsilon}$.

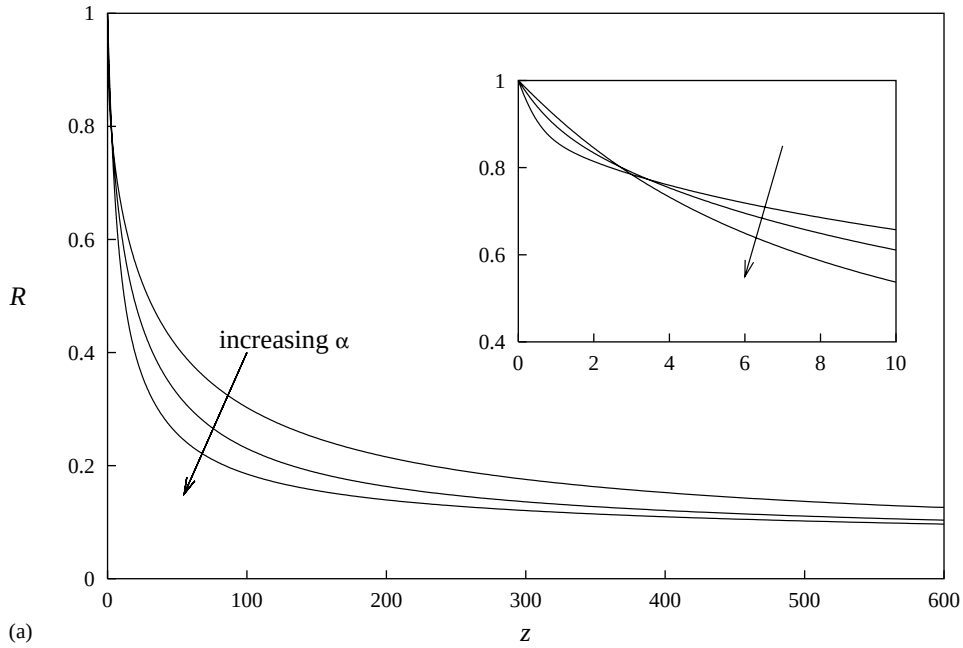

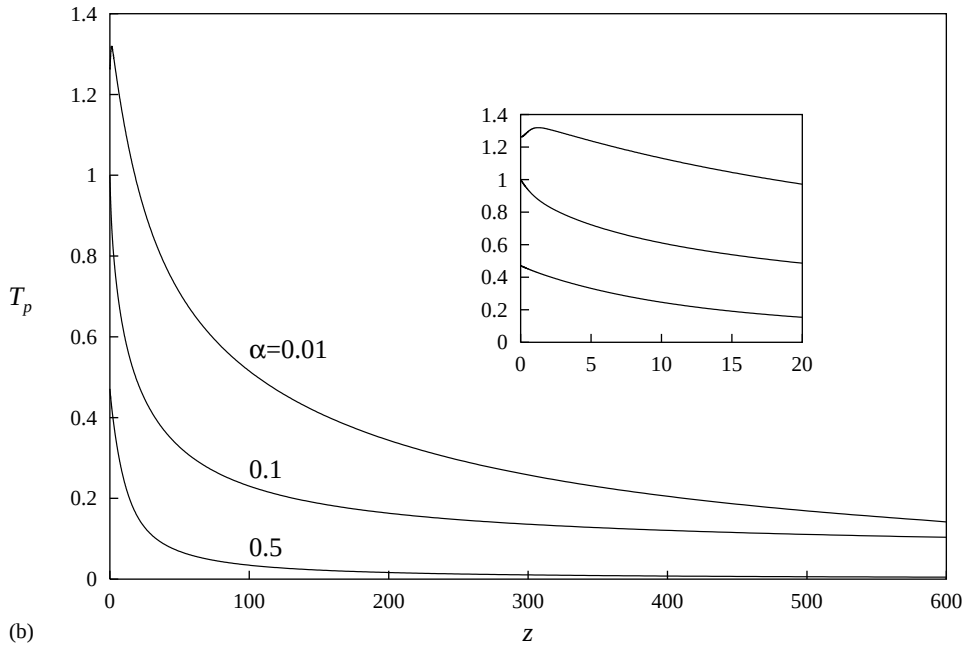

Fig. 5. Predictions of the 1D theory for three values of α: 0.01, 0.1 and 0.5 with other parameters fixed at those of Fig. 4: (a) jet radius $R(z)$; (b) polymer tensile force $T_{\mathrm{p}}(z)$. The insets show details near the nozzle.

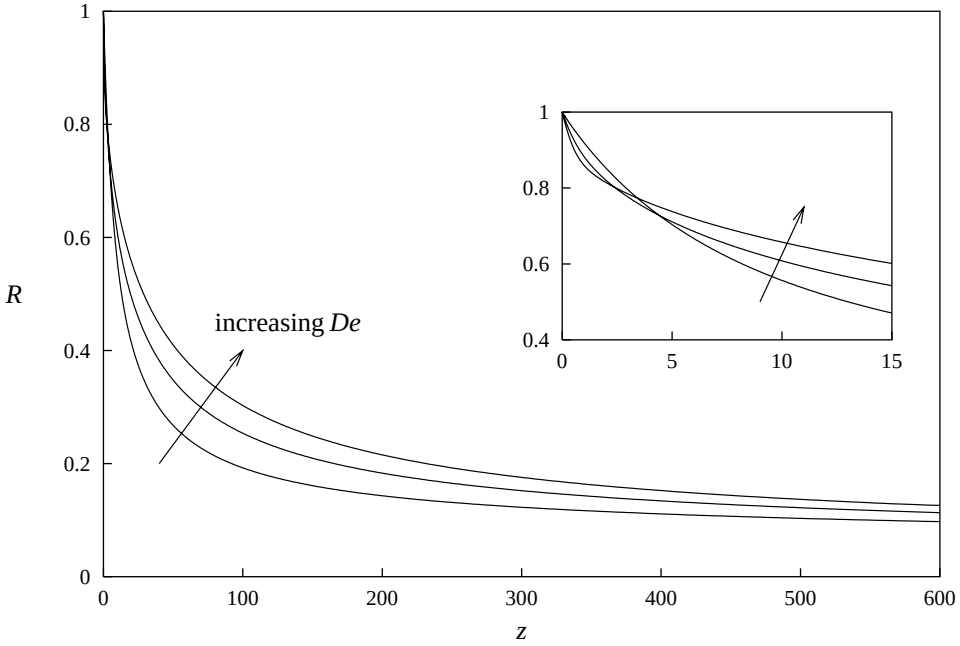

Fig. 6. $R(z)$ profiles for $De = 1$, 5 and 10 with other parameters fixed at those of Fig. 4.

Inspection of $v'(z)$ profiles shows that a higher *De* indeed corresponds to a larger v' in the first few radii of the jet. As a result, $\bar{\eta}^+$ initially grows more rapidly with z for larger *De*, and that explains the effect in Fig. 6. Because the extension never attains steady state in a Lagrangian sense, it is not possible to positively identify the role of extension-thickening in Fig. 6. In the latter half of the jet where v' varies relatively slowly, extension-thickening probably has contributed to arresting jet stretching for larger *De*. One may note the resemblance between decreasing α in Fig. 5(a) and increasing *De* in Fig. 6. However, the latter stems from a distinct rheological effect (cf. Fig. 3(b)) not included in the empirical Eq. (1).

Finally, Fig. 7 illustrates the effect of the solvent by varying r_η while keeping the total viscosity η_0 fixed. Since a larger r_η implies more polymer contribution to the stress, the effect of strain-hardening is more pronounced: stretching is intensified initially but suppressed downstream.

4. Comparison with experiment

The thinning curve $R(z)$ is relatively easy to measure in the laboratory, but comparison between model prediction and measurement is hampered to some degree by the fact that no single study has reported all the material and operating parameters. In Fig. 8, we have chosen to compare the predicted jet radius $R(z)$ with the measurement of Doshi and Reneker [26] for a 4% PEO solution. Doshi and Reneker [26] give three parameters: the electric field ($E_\infty = 40\,\mathrm{kV\,m^{-1}}$), the nozzle radius ($R_0 = 45\,\mu\mathrm{m}$) and the length of the straight jet ($L = 30\,\mathrm{mm}$). The density and dielectric constant are found in Hohman et al. [2]: $\rho = 1.2 \times 10^3\,\mathrm{kg\,m^{-3}}$, $\epsilon/\bar{\epsilon} = 42.7$. Fong et al. [27] have provided additional material properties for a 4% PEO solution: viscosity $\eta_0 = 12.5\,\mathrm{P}$; surface tension $\gamma = 76.6\,\mathrm{dyn\,cm^{-1}}$, and conductivity

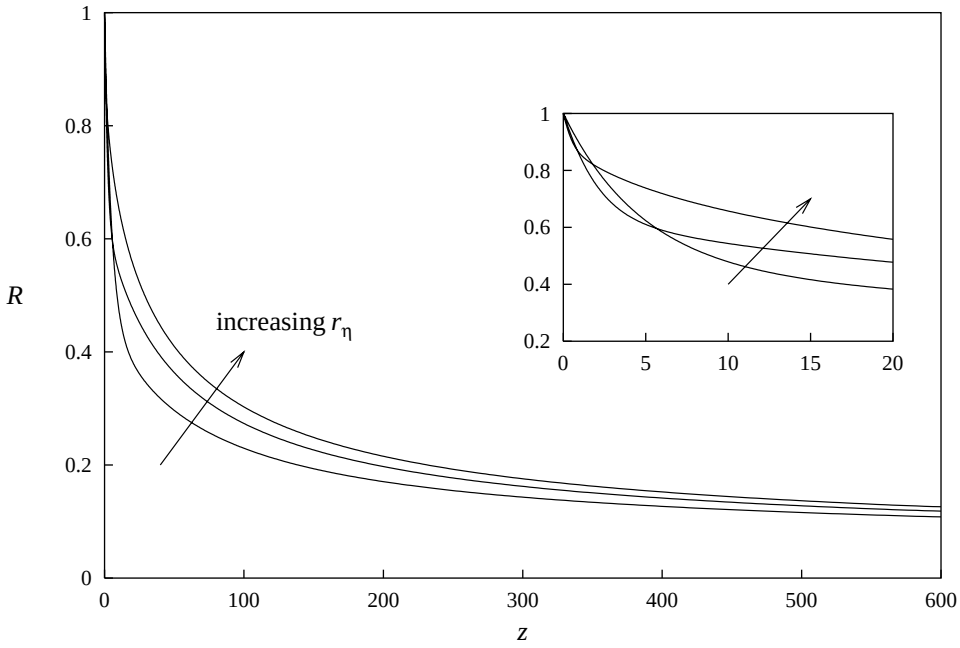

Fig. 7. $R(z)$ profiles for $r_\eta = 0.2$, 0.5 and 0.9 with other parameters fixed at those of Fig. 4.

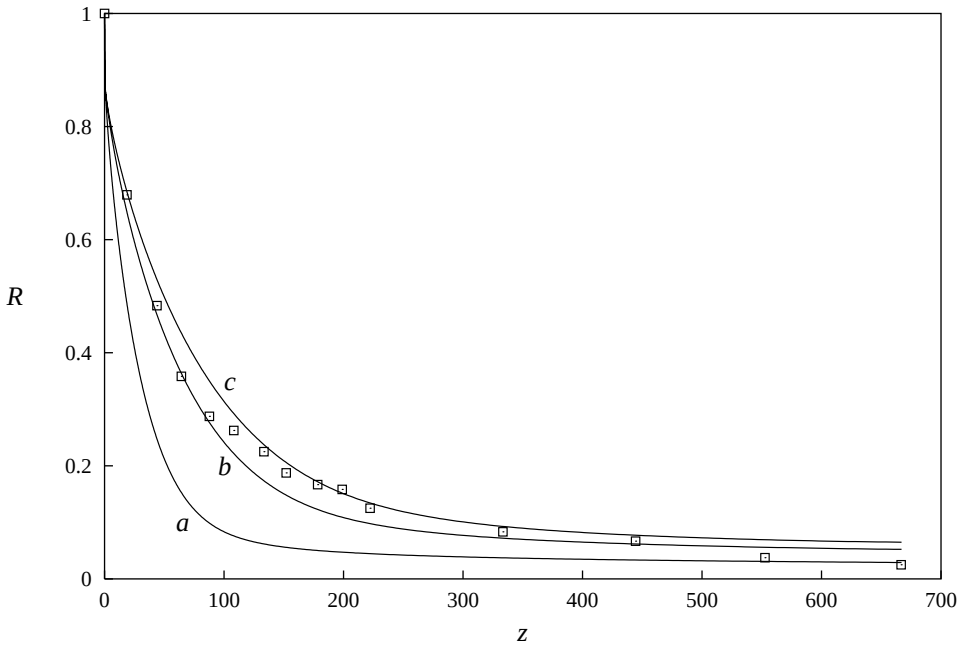

Fig. 8. Comparison of our model predictions with the experimental data of Doshi and Reneker [26] for a 4% PEO solution. The theoretical curves a, b and c correspond to flow rates $Q = 10$, 20 and 25 μl min^{-1}. Other parameters are given in the text.

$K = 4.902 \times 10^{-3}\,\Omega^{-1}\,\mathrm{m}^{-1}$. The solvent viscosity is $\eta_s = 10^{-2}$ poise for water. The relaxation time of concentrated solutions and melts ranges from 1 s to hundreds of seconds ([28], pp. 342–345), and we have assumed $\lambda = 10$ s. Since the strain-rate is exceedingly high, *De* is easily in the thousands. Thus, the polymer stretches elastically and the exact value of *De* (or λ) has little effect on the model prediction. We have chosen $\alpha = 0.01$ since it produces strain-hardening of roughly two orders of magnitude (cf. Fig. 3(a)), comparable to data for concentrated solutions and melts [8].

As for operating parameters, Fong and Reneker [29] have plotted I and Q as functions of the applied field for a 2.44% PEO solution in the following ranges: $0.1\,\mu\mathrm{A} < I < 6\,\mu\mathrm{A}$, $10\,\mu\mathrm{l\,min}^{-1} < Q < 80\,\mu\mathrm{l\,min}^{-1}$. The electric field used by Doshi and Reneker [26] corresponds to $I = 0.12\,\mu\mathrm{A}$, $Q = 10\,\mu\mathrm{l\,min}^{-1}$. For these parameters, our model overpredicts the thinning of the jet (curve a in Fig. 8). Increasing the flow rate Q to 20 or $25\,\mu\mathrm{l\,min}^{-1}$ shifts the prediction closer to experimental data (curves b and c). A more rigorous test of the model is not possible since the Q and I values in [29] are for a 2.44% solution while the measured $R(z)$ is for a 4% solution. Nonetheless, the data being enveloped by model predictions over a reasonable range of Q lends some confidence to the model in qualitative terms. In addition, Hohman et al. [2] have shown that details of the experimental setup, such as the protrusion of the nozzle, can influence the jet greatly. Such features are not explicitly accounted for in our model, but are implicitly incorporated, to some degree, via the parameters $E(0)$, Q and I. We have found no systematic measurements of the effects of rheological parameters on electrospinning to validate model predictions in Figs. 5–7.

In summary, we have incorporated the Giesekus model into a 1D slender-body theory and examined the role of nonlinear rheology in the stretching of an electrically charge jet. Strain-hardening promotes jet thinning at the beginning but suppresses it further downstream to produce thicker fibers. This prediction of the Giesekus model confirms that of the empirical model employed in [6]. In addition, the Giesekus model also predicts earlier onset of strain-hardening at higher strain rate. Though definitive comparison with experiments cannot be made, the theory appears to predict jet thinning on the right order of magnitude. The behavior of the jet forms an interesting contrast to its counterpart in conventional fiber spinning.

Acknowledgements

This work was supported in part by 3M, PSC-CUNY and the NSF through a Career Award. I thank Morton Denn for stimulating discussions and the referees for valuable criticism and suggestions.

References

[1] D.H. Reneker, I. Chun, Nanometre diameter fibres of polymer, produced by electrospinning, Nanotechnology 7 (1996) 216–223.
[2] M.M. Hohman, M. Shin, G. Rutledge, M.P. Brenner, Electrospinning and electrically forced jets. I. Stability theory. II. Applications, Phys. Fluids 13 (2001) 2201–2236.
[3] A.F. Spivak, Y.A. Dzenis, Asymptotic decay of radius of a weakly conductive viscous jet in an external electric field, Appl. Phys. Lett. 73 (1998) 3067–3069.
[4] D.H. Reneker, A.L. Yarin, H. Fong, S. Koombhongse, Bending instability of electrically charged liquid jets of polymer solutions in electrospinning, J. Appl. Phys. 87 (2000) 4531–4547.
[5] A.L. Yarin, S. Koombhongse, D.H. Reneker, Bending instability in electrospinning of nanofibers, J. Appl. Phys. 89 (2001) 3018–3026.
[6] J.J. Feng, The stretching of an electrified non-Newtonian jet: a model for electrospinning, Phys. Fluids 14 (2002) 3912–3926.

[7] V. Tirtaatmadja, T. Sridhar, A filament stretching device for measurement of extensional viscosity, J. Rheol. 37 (1993) 1081–1102.
[8] R.B. Bird, C.F. Curtiss, R.C. Armstrong, O. Hassager, Dynamics of Polymeric Liquids, vol. 1, Fluid Mechanics, Wiley, New York, 1987.
[9] H. Giesekus, A simple constitutive equation for polymeric fluids based on the concept of configuration-dependent tensorial mobility, J. Non-Newtonian Fluid Mech. 11 (1982) 69–109.
[10] S.A. Khan, R.G. Larson, Comparison of simple constitutive equations for polymer melts in shear and biaxial and uniaxial extensions, J. Rheol. 31 (1987) 207–234.
[11] V. Tirtaatmadja, T. Sridhar, Comparison of constitutive equations for polymer solutions in uniaxial extension, J. Rheol. 39 (1995) 1133–1160.
[12] D.A. Saville, Electrohydrodynamics: the Taylor–Melcher leaky dielectric model, Ann. Rev. Fluid Mech. 29 (1997) 27–64.
[13] J. Eggers, T.F. Dupont, Drop formation in a one-dimensional approximation of the Navier–Stokes equation, J. Fluid Mech. 262 (1994) 205–221.
[14] X. Zhang, R.S. Padgett, O.A. Basaran, Nonlinear deformation and breakup of stretching liquid bridges, J. Fluid Mech. 329 (1996) 207–245.
[15] M.M. Denn, Fibre spinning, in: J.R.A. Pearson, S.M. Richardson (Eds.), Computational Analysis of Polymer Processing, Applied Science Publishers, New York, 1983 (Chapter 6).
[16] A.M. Ganan-Calvo, Cone-jet analytical extension of Taylor's electrostatic solution and the asymptotic universal scaling laws in electrospraying, Phys. Rev. Lett. 79 (1997) 217–220; Erratum 85 (2000) 4193.
[17] L.T. Cherney, Structure of Taylor cone-jets: limit of low flow rates, J. Fluid Mech. 378 (1999) 167–196.
[18] V.N. Kirichenko, I.V. Petryanov-Sokolov, N.N. Suprun, A.A. Shutov, Asymptotic radius of a slightly conducting liquid jet in an electric field, Sov. Phys. Dokl. 31 (1986) 611–613.
[19] M.M. Denn, C.J.S. Petrie, P. Avenas, Mechanics of steady spinning of a viscoelastic liquid, AIChE J. 21 (1975) 791–799.
[20] R.J. Fisher, M.M. Denn, A theory of isothermal melt spinning and draw resonance, AIChE J. 22 (1976) 236–246.
[21] T.C. Papanastasiou, C.W. Macosko, L.E. Scriven, Z. Chen, Fiber spinning of viscoelastic fluid, AIChE J. 33 (1987) 834–842.
[22] W.H. Press, S.A. Teukolsky, W.T. Vetterling, B.P. Flannery, Numerical Recipes in Fortran 77, second ed., Cambridge University Press, New York, 1992.
[23] H.M. Laun, H. Münstedt, Elongational behavior of a low density polyethylene melt, Rheol. Acta 17 (1978) 415–425.
[24] G.I. Taylor, Disintegration of water drops in an electric field, Proc. R. Soc. Lond. A280 (1964) 383–397.
[25] R.I. Tanner, Engineering Rheology, second ed., Oxford University Press, New York, 2000.
[26] J. Doshi, D.H. Reneker, Electrospinning and applications of electrospun fibers, J. Electrostat. 35 (1995) 151–160.
[27] H. Fong, I. Chun, D.H. Reneker, Beaded nanofibers formed during electrospinning, Polymer 40 (1999) 4585–4592.
[28] R.B. Bird, C.F. Curtiss, R.C. Armstrong, O. Hassager, Dynamics of Polymeric Liquids, vol. 2, Kinetic Theory, Wiley, New York, 1987.
[29] H. Fong, D.H. Reneker, Electrospinning and the formation of nanofibers, in: D.R. Salem (Ed.), Structure Formation in Polymeric Fibers, Hanser Publishers, Munich, 2001 (Chapter 6).